

Genetic requirement for *Mycl* and efficacy of RNA Pol I inhibition in mouse models of small cell lung cancer

Dong-Wook Kim,^{1,14} Nan Wu,^{2,3,14} Young-Chul Kim,⁴ Pei Feng Cheng,⁵ Ryan Basom,⁶ Dongkyoon Kim,⁷ Colin T. Dunn,¹ Anastasia Y. Lee,¹ Keebeom Kim,¹ Chang Sup Lee,¹ Andrew Singh,¹ Adi F. Gazdar,^{8,9,10} Chris R. Harris,^{11,12,13} Robert N. Eisenman,⁵ Kwon-Sik Park,^{1,15} and David MacPherson^{2,3,15}

¹Department of Microbiology, Immunology, and Cancer Biology, University of Virginia School of Medicine, Charlottesville, Virginia 22908, USA; ²Division of human Biology, ³Division of Public Health Sciences, Fred Hutchinson Cancer Research Center, Seattle, Washington 98109, USA; ⁴Department of Biostatistics and Bioinformatics, Moffitt Cancer Center, Tampa, Florida 33612, USA; ⁵Basic Sciences Division, ⁶Genomics and Bioinformatics Shared Resource, Fred Hutchinson Cancer Research Center, Seattle, Washington 98109, USA; ⁷Stanford University Institute for Stem Cell Biology and Regenerative Medicine, Palo Alto, California 94305, USA; ⁸Hamon Center for Therapeutic Oncology Research, ⁹Simmons Cancer Center, ¹⁰Department of Pathology, University of Texas Southwestern Medical Center, Dallas, Texas 75390, USA; ¹¹Raymond and Beverly Sackler Foundation, New Brunswick, New Jersey 08901, USA; ¹²Rutgers Cancer Institute of New Jersey, New Brunswick, New Jersey 08903, USA; ¹³Department of Pediatrics, Robert Wood Johnson Medical School, New Brunswick, New Jersey 08901, USA

Small cell lung cancer (SCLC) is a devastating neuroendocrine carcinoma. *MYCL* (L-Myc) is frequently amplified in human SCLC, but its roles in SCLC progression are poorly understood. We isolated preneoplastic neuroendocrine cells from a mouse model of SCLC and found that ectopic expression of L-Myc, c-Myc, or N-Myc conferred tumor-forming capacity. We focused on L-Myc, which promoted pre-rRNA synthesis and transcriptional programs associated with ribosomal biogenesis. Deletion of *Mycl* in two genetically engineered models of SCLC resulted in strong suppression of SCLC. The high degree of suppression suggested that L-Myc may constitute a therapeutic target for a broad subset of SCLC. We then used an RNA polymerase I inhibitor to target rRNA synthesis in an autochthonous *Rb/p53*-deleted mouse SCLC model and found significant tumor inhibition. These data reveal that activation of RNA polymerase I by L-Myc and other MYC family proteins provides an axis of vulnerability for this recalcitrant cancer.

[*Keywords:* oncogene; progression; neuroendocrine; transcription factor; ribosome biogenesis]

Supplemental material is available for this article.

Received February 10, 2016; revised version accepted May 5, 2016.

Small cell lung cancer (SCLC) is an aggressive highly metastatic neuroendocrine carcinoma that represents 10%–15% of lung cancer cases. Treatments for SCLC have not significantly improved over the last four decades, and there are no currently approved targeted therapies. It is therefore essential that the biology of major genes that drive SCLC be linked to novel therapeutic approaches. Sequencing of human SCLC has identified a panel of mutant genes (Rudin et al. 2012; George et al. 2015), but, to date, easily druggable mutant gene targets for SCLC have not been identified.

Prevalent genetic alterations in SCLC include near-universal *RB* and *p53* deletion and frequent amplification of

MYC family members: *MYCL* (L-Myc), *MYCN* (N-Myc), or *MYC* (c-Myc) (Johnson et al. 1987; George et al. 2015). MYC proto-oncogenes are basic helix–loop–helix (bHLH) leucine zipper transcription factors that heterodimerize with their partner, MAX, and bind to E-box elements. MYC family members can also mediate gene repression, confer global effects on transcriptional elongation, control global chromatin organization, and promote ribosomal biogenesis and protein synthesis (for review, see Dang 2012). In SCLC, *MYCL* amplifications are most frequent, but *MYCN* or *MYC* amplifications also occur, and these events are mutually exclusive, suggesting shared critical

¹⁴These authors contributed equally to this work.

¹⁵These authors contributed equally to this work.

Corresponding authors: dmacpher@fhcrc.org, kp5an@virginia.edu

Article is online at <http://www.genesdev.org/cgi/doi/10.1101/gad.279307.116>.

© 2016 Kim et al. This article is distributed exclusively by Cold Spring Harbor Laboratory Press for the first six months after the full-issue publication date (see <http://genesdev.cshlp.org/site/misc/terms.xhtml>). After six months, it is available under a Creative Commons License (Attribution-NonCommercial 4.0 International), as described at <http://creativecommons.org/licenses/by-nc/4.0/>.

oncogenic function (Johnson et al. 1987; George et al. 2015). Cloned three decades ago based on frequent amplification and high expression in SCLC (Nau et al. 1985), *MYCL* is the least understood of the oncogenic *MYC* members. *MYCL* has a much lower degree of transforming activity relative to *MYC* or *MYCN* (Birrer et al. 1988; Barrett et al. 1992), although *MYCL* can replace *MYC* as a factor that promotes cell reprogramming in producing induced pluripotent stem cells (iPSCs) (Nakagawa et al. 2010). In contrast to *Mycn* and *Myc*, which are required for embryonic development, genetic inactivation of *Mycl* in the germline of mice is viable without notable phenotypes (Hatton et al. 1996). Except for a recently discovered specific role in dendritic cells of the immune system (Kc et al. 2014), biological roles for *Mycl* in vivo have remained elusive. Thus, despite *MYCL* being the major amplified family member in SCLC, in vivo roles for *MYCL* in the cells that give rise to SCLC have not been investigated.

In vivo overexpression studies using a mouse model demonstrated that *MYCL* can promote SCLC (Huijbers et al. 2014), but it is still unknown how this is mediated and whether *MYCL*-driven biological activities constitute therapeutic targets. Major questions about oncogenic functions of *MYCL* exist. Most important clinically is whether an understanding of *MYCL*-driven protumorigenic pathways can be leveraged to improve therapies for SCLC. The lack of adverse effects of *Mycl* deletion on normal physiology in mice suggests that targeting *Mycl* therapeutically could be relatively specific for tumor cells, but we need to better understand how *MYCL* promotes SCLC. One biological process that *MYC* members control is ribosomal biogenesis and protein synthesis (van Riggelen et al. 2010). Of the family members, this has been best studied for c-*MYC*, which controls the activity of RNA polymerase I (Pol I), Pol II, and Pol III, promoting ribosomal rRNA synthesis and ribosomal protein expression (Dang 2012). Whether this axis represents a vulnerability associated with L-*Myc* in SCLC is unknown.

In this study, we used a novel cellular system that is based on transformation of preneoplastic lung neuroendocrine cells to explore driver genes such as L-*Myc*. We also used mouse genetics across multiple models to show that inactivation of *Mycl* dramatically suppresses SCLC in vivo. Moreover, our work points to a therapeutic approach that exhibits efficacy in mouse models of SCLC as monotherapy.

Results

Isolation of preneoplastic precursors of SCLC (preSCs)

To characterize precursor cells of SCLC, we developed a BAC transgenic strain (*Chga-GFP*) that expresses green fluorescence protein (GFP) under the control of 190 kbs of genomic sequences flanking the *Chga* locus (Fig. 1A; Supplemental Fig S1). GFP-positive pulmonary neuroendocrine cells (PNEC) in this strain were specifically labeled as demonstrated using immunostaining to the neuroendocrine marker CGRP (Fig. 1A) and isolated using

fluorescence-activated cell sorting (FACS). We sorted the GFP-positive population from *Chga-GFP* mice (~100 cells could be sorted from three to four mice) and detected viable cells after sorting. However, the cells did not proliferate and started dying after 3–5 d in culture (Supplemental Fig. S2A). To investigate the potential role of these cells in SCLC, we crossed the *Chga-GFP* mice with *Rb^{lox/lox}; p53^{lox/lox}; p130^{lox/lox}* mice and initiated SCLC via intratracheal instillation of Ad-CMV-Cre (Schaffer et al. 2010). This *Rb/p53/p130*-deleted mouse model recapitulates key features of human SCLC, including neuroendocrine characteristics and metastatic spread (Schaffer et al. 2010; Gazdar et al. 2015). One month after Cre delivery, at which time macroscopic lesions were not yet evident, we isolated a small number of GFP-positive cells from the lungs of *Chga-GFP; Rb^{lox/lox}; p53^{lox/lox}; p130^{lox/lox}* mice using FACS (Fig. 1B). We also isolated SCLC tumor cells in a similar fashion at 6 mo after Cre delivery, a time point when extensive SCLC is present in the *Rb^{lox/lox}; p53^{lox/lox}; p130^{lox/lox}* model (Fig. 1B). The GFP cells from early stages of tumorigenesis grew as a monolayer attached to the culture dish, whereas mouse SCLC cells formed spheres or aggregates and grew in suspension or loosely attached to the culture dish. The GFP-positive cells continued to proliferate in RPMI1640 medium supplemented with 10% bovine growth serum but did not form subcutaneous tumors in immune-deficient nude mice. In contrast, when introduced in the same number, the GFP-positive mouse SCLC tumor cells readily formed palpable tumors (Fig. 1C). The cells derived at 1 mo after Adeno-Cre (Ad-Cre) delivery, an early stage of tumor development, acquired unlimited replicative potential, likely owing to deletion of both the *Rb* and *p53* genes, a common cause of cell immortalization. However, they were not yet tumorigenic, possibly owing to the lack of other key oncogenic factors being activated. We refer to these mutant neuroendocrine cells as preSCs. Genotyping PCR and RT-qPCR showed deletion of targeted *Rb* and *p53* exons and expression of various neuroendocrine cell markers, including *Ncam1*, *Chga*, *Syp*, *Cgrp*, and *Ascl1*, in both the preSC and SCLC cells (Fig. 1D,E; Supplemental Fig S2B). The preSC cells also maintained normal levels of *E-Cadherin* relative to normal lungs, while the SCLC cells exhibited lower E-Cadherin levels. Moreover, while bulk preSC cells did not express detectable *Mycl*, the SCLC cells exhibited high levels of *Mycl* expression (Fig. 1E). In addition, higher levels of *Mycn* and lower levels of *Myc* were observed in preSC cells and SCLC cells relative to normal lung tissue (Fig. 1E).

L-*Myc* drives tumorigenic progression of preSCs

We hypothesized that perturbing preSCs would allow us to test roles for candidate oncogenes and tumor suppressor genes in SCLC. One of the most prevalent oncogenic events in SCLC is amplification of *MYCL*, and we observed sharply increased expression of *Mycl* in SCLC relative to preSCs in our model (Fig. 1E). To delineate roles for L-*Myc* in promoting SCLC, we first studied the effect of L-*Myc* overexpression in preSCs using a retroviral

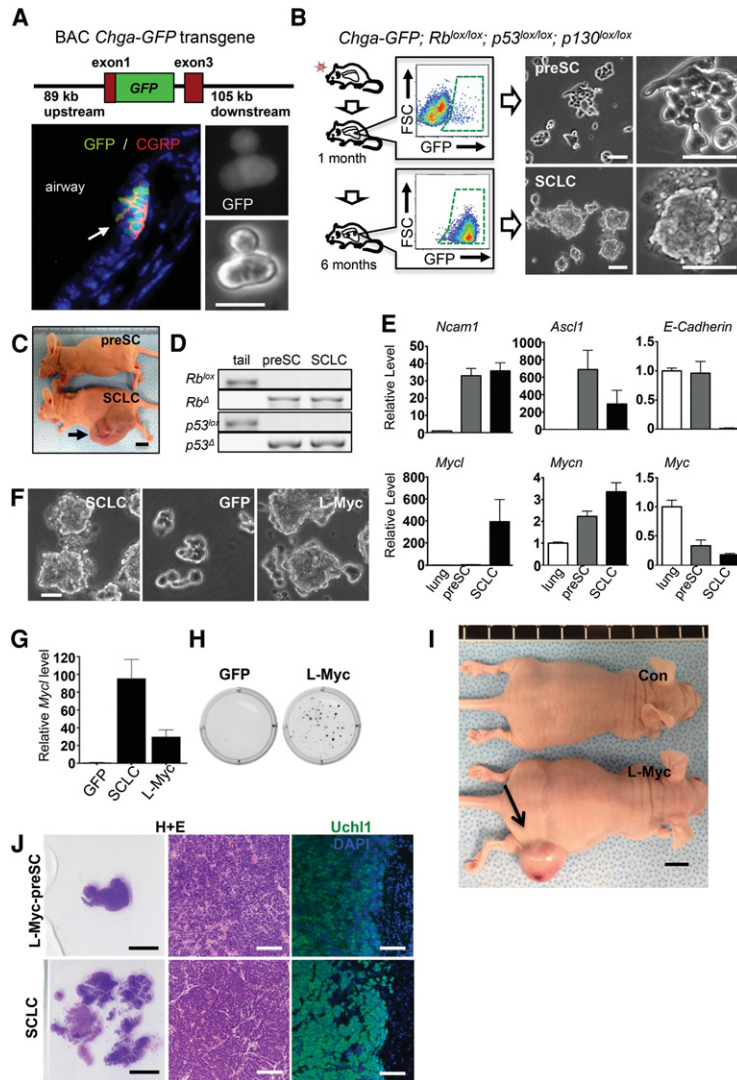


Figure 1. L-Myc converts preneoplastic lung neuroendocrine cells to SCLC. (A, top) Diagram of the *Chga-GFP* transgene. (Bottom left) PNECs (arrow) in *Chga-GFP* mice stained for Calcitonin gene-related peptide (CGRP) (red signal) with positive staining overlapping with *Chga-GFP*. (Bottom right) GFP immunofluorescence (top) and phase-contrast (bottom) images of PNECs isolated by FACS. (B) Strategy to isolate preSCs and tumor cells using FACS. The dotted green line highlights GFP-positive cells. (Right) Images of preSC and SCLC cells. (C) Nude mice 1 mo after injection of preSC or SCLC cells. The arrow points to the tumor. (D) Genotyping PCR showing deletion of *Rb* and *p53* in preSC and SCLC tumor cells. (E) RT-qPCR data showing *Myc* member expression and neuroendocrine markers in normal lung (lung), preSC, and SCLC cells. $n = 3$. Data were normalized to levels of ARBP P0 and expressed relative to expression in normal lung cells. (F) Images of mouse SCLC cells compared with preSCs infected with the retroviruses expressing GFP or L-Myc. $n = 3$. (G) RT-qPCR data showing expression of L-Myc normalized to ARBP P0 in SCLC cells or preSCs infected with GFP or L-Myc. $n = 3$. (H) Results of soft agar assay. $n = 3$. (I) Nude mice 1 mo after injection of cells infected with retro-GFP or L-Myc. Arrow points to the tumor. (J) Hematoxylin and eosin (H&E) and Uchl1 (Pgp9.5) staining of mouse SCLC cells or L-Myc preSCs. Bars: A, B, 10 μm ; C, 1 cm; F, 10 μm ; I, 1 cm; J, far left, 0.5 cm; J, 100 μm .

vector. In <2 wk, the preSCs infected with retroviral L-Myc (L-Myc-preSCs) formed spheres typical of both human SCLC and mouse SCLC cells in culture (Fig. 1F). Transition from adherent cell culture to sphere formation indicates loss of contact inhibition and anchorage independence, two of the hallmarks of cancer cells. Additionally, the L-Myc-preSC cells formed colonies in soft agar (Fig. 1H) and palpable tumors with typical SCLC morphology in the flanks of athymic nude mice (Fig. 1I), whereas the control preSCs infected with retroviral GFP were morphologically the same as uninfected cells and failed to form palpable tumors in nude mice. In human SCLC, *MYCL*, *MYCN*, or *MYC* can be amplified in a mutually exclusive manner, suggesting that key oncogenic activities may be shared among these family members. Similar to L-Myc, the retroviral expression of N-Myc or c-Myc also transformed preSCs, and the resulting phenotypes in culture and allograft experiments were almost identical to those caused by L-Myc (Supplemental Fig. S2C,D). Expression of L-Myc or N-Myc in each group of transformed cells is dramatically higher (40-fold to 60-fold

than control preSCs, but c-Myc levels in the c-Myc-preSCs is increased only about threefold to fourfold (Fig. 1G; Supplemental Fig S2E). Notably, higher *MYC* expression (~20-fold increase) caused morphological changes of spheroid cells into multigonal, attached cells (Supplemental Fig. S2C). The allograft tumors generated from the preSC-expressing *MYC* family genes showed histological features of SCLC in hematoxylin and eosin (H&E) staining and also stained for neuroendocrine markers, including Calcitonin gene-related peptide (CGRP) and UCHL1 (Fig. 1J; Supplemental Fig S2F). Thus, this novel system revealed that overexpression of L-Myc, N-Myc, or c-Myc is sufficient to drive a transition from preneoplastic to neoplastic SCLC.

Mycl inactivation suppresses SCLC

To determine whether *Mycl* is required for SCLC development, we used a floxed allele for *Mycl* generated by inserting loxP sites upstream of the first exon and downstream from exon 3. We conditionally inactivated *Mycl* at the

time of tumor initiation in two different highly penetrant mouse models of SCLC. In the first cross, we used a model in which intratracheal Ad-Cre (Ad-CMV-Cre) drives deletion of *Rb^{lox/lox};p53^{lox/lox};p130^{lox/lox}* alleles in the lung epithelium, in which SCLC, often with a large cell neuroendocrine component, rapidly arises from expanding neuroendocrine cells (Schaffer et al. 2010; Gazdar et al. 2015). Human SCLC almost always exhibits *RB/P53* deletion and occasionally *RBL2/130* deletion (George et al. 2015). We bred the *Mycl* floxed allele into the model, allowing us to compare littermate *Rb^{lox/lox};p53^{lox/lox};p130^{lox/lox}* mice that were *Mycl^{+/+}*, *Mycl^{+/lox}*, or *Mycl^{lox/lox}*. Six months after Ad-CMV-Cre infection, we analyzed the lungs of the infected mice. The mice with homozygous *Mycl* floxed alleles exhibited drastically reduced tumor burden compared with those with wild-type or heterozygous floxed alleles (Fig. 2A). Genotyping PCR using primers for floxed or wild-type *Mycl* alleles confirmed robust recombination of the floxed allele in the lung tumors of littermates (Supplemental Fig. S3A). Histology and immunostaining showed that the tumors and lesions with each genotype exhibit well-known SCLC features, including scanty cytoplasm and positive staining for Uchl1 and CGRP (Supplemental Fig. S3B). The decrease in tumor burden correlated significantly with lower rates of proliferation, as measured by quantification of cells positive for phosphorylated histone H3 (pHH3) (Fig. 2B), but not with higher rates of cell death (data not shown).

To determine whether the importance of *Mycl* is broadly relevant to SCLC of differing genotypes, we also deleted *Mycl* in a mouse model driven by *Rb/p53* and *Pten* deletion. The PTEN pathway is altered through inactivating deletions/mutations in *PTEN* or activating mutations in *PIK3CA* in a subset of human SCLC cells. In this mouse model, *Rb^{lox/lox};p53^{lox/lox};Pten^{lox/lox}* mice were infected intratracheally with Ad-Cre driven by a neuroendocrine (Calcitonin/CGRP) promoter (Ad-CGRP-Cre) (as in Sutherland et al. 2011; McFadden et al. 2014). The Ad-CGRP-Cre approach was taken because combined deletion of *Rb/p53/Pten* throughout the lung using the more widely active Ad-CMV-Cre leads to substantial adenocarcinoma that impairs study of SCLC (Cui et al. 2014). When mice were examined 4 mo following Ad-CGRP-Cre delivery, we found clear reductions in number and size of early tumors in the *Mycl*-deleted model (Fig. 2C). In a long-term survival study, Kaplan-Meier analysis revealed striking suppression of SCLC in the absence of *Mycl* ($P=0.0005$, log rank test) (Fig. 2D). Indeed, ~40% of the animals in the *Mycl^{lox/lox}* cohort were free of tumors when euthanized at the end of study at 380 d. While Ad-CGRP-Cre *Rb/p53/Pten^{lox/lox}* mice developed SCLC as the major phenotype, with occasional small foci of adenocarcinoma, increased heterogeneity in tumor spectrum with additional tumor types beyond SCLC was apparent upon *Rb/p53/Pten* and *Mycl* inactivation (Fig. 2E). For example, SCLC and adenosquamous carcinoma were found in one case; in another, SCLC and adenocarcinoma were found. We cannot rule out the possibility of leakiness in the Ad-CGRP-Cre system, and one *Rb/p53/Pten/Mycl* animal developed adenocarcinoma in the

absence of SCLC. Increased heterogeneity in *Mycl*-deficient tumors may be a consequence of the longer time that these mice had to develop tumors (Fig. 2D), and this increased heterogeneity in tumor spectrum was not apparent at the 4-mo time point (Fig. 2C). We also examined MYC family member copy number in *Rb/p53/Pten* versus *Rb/p53/Pten/Mycl* SCLC cells using real-time PCR. One of 10 SCLCs from the *Rb/p53/Pten* AdCGRP Cre model exhibited *Mycl* amplification with no *Mycn* amplifications found, while one of eight SCLCs in the *Rb/p53/Pten/Mycl* model exhibited *Mycn* amplification (Supplemental Fig. S3C). These genetic data indicate that *Mycl* inactivation strongly suppresses SCLC and suggest that pharmacologic inhibition of L-Myc or its downstream effectors could be a broad approach to treating SCLC, even in tumors without MYCL amplification.

Tumor inhibition in the *Rb/p53/p130* and *Rb/p53/Pten* mouse models precluded characterizing a continued role for *Mycl* in late stage tumor cells. Thus, to test roles of *Mycl* in cells derived from SCLC, we acutely ablated *Mycl* function in *Rb/p53*-deleted mouse SCLC cell lines using CRISPR/Cas9-mediated gene targeting. Targeting *Mycl* reduced the ability of targeted cells to form colonies in soft agar compared with controls (Fig. 2F,G). These results indicate that *Mycl* is important for continuing growth of the tumor cells in culture (Fig. 2F,G). Targeting *Mycn* also reduced the colony-forming capacity of tumor cells, whereas CRISPR inactivation of *Myc* did not lead to significant changes in colony formation (Fig. 2F,G). We validated CRISPR-mediated frameshift mutations of the MYC family genes by sequencing the genome of mouse lung fibroblast cells, which were targeted with the same vector but not affected (Supplemental Fig. S3D). The inhibitory effect of targeting *Mycl* and *Mycn* in mouse SCLC cells was congruent with their high expression in mouse SCLC cells relative to normal lung cells (Fig. 1E). The lack of inhibitory effect of targeting *Myc* on cell growth was associated with lower levels of *Myc* relative to normal lung cells (Fig. 1E). Thus, in contrast to *Mycl*, basal levels of *Myc* expression may be unimportant for the long-term growth of SCLC cells even though overexpression of *Myc* promoted SCLC (Supplemental Fig. S2D).

Identification of effector pathways underlying L-Myc-induced SCLC progression

Our results support the concept of L-Myc inhibition as a strategy for therapy and prevention of SCLC. Given the lack of a direct inhibitor of L-Myc, however, we explored effectors of the L-Myc-driven oncogenic pathway as alternative targets. To identify potential L-Myc-driven oncogenic pathways, we compared genome-wide gene expression profiles of control preSCs and L-Myc-preSCs using Affymetrix microarrays. Using two gene expression analysis platforms that use different statistical methods, including limma (linear models for microarray data) and LPE (local pooled error), we identified a set of 1017 annotated genes differentially expressed between the preSCs and L-Myc-preSCs and defined the gene set as the L-MYC signature. A list of the top 20 up-regulated and

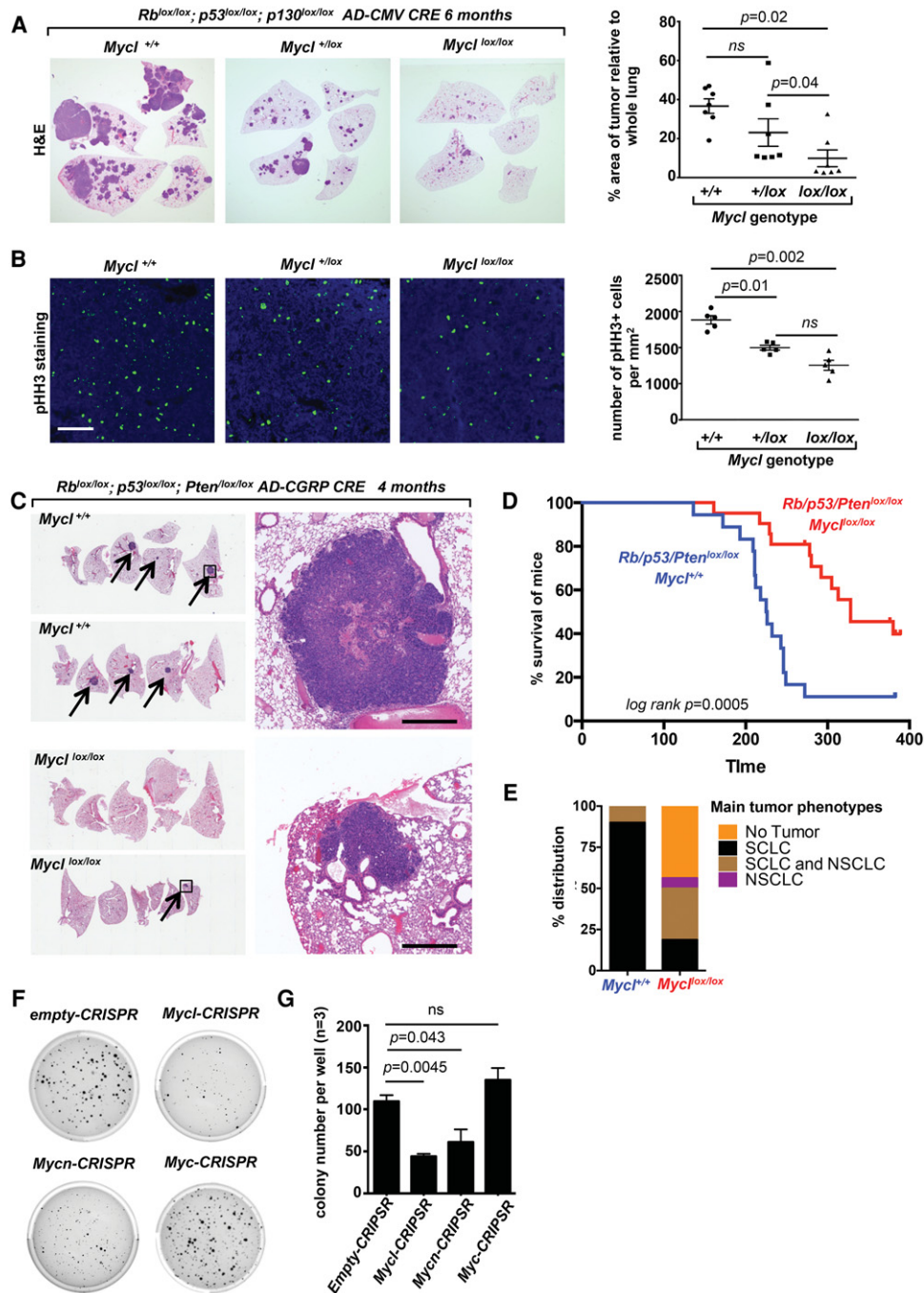


Figure 2. Deletion of *Mycl* suppresses SCLC. (A) H&E staining of *Rb^{lox/lox}; p53^{lox/lox}; p130^{lox/lox}* mouse lungs either *Mycl^{+/+}*, *Mycl^{+/lox}*, or *Mycl^{lox/lox}* 6 mo after Ad-CMV-Cre treatment. (Right) Tumor area quantification. (B) pHH3 staining showing reduced proliferation in *Rb/p53/p130* mice that were *Mycl^{lox/lox}* compared with *Mycl^{+/+}*. (Right) Quantification of pHH3-positive cells. (C) H&E staining of *Rb^{lox/lox}; p53^{lox/lox}; Pten^{lox/lox}* mouse lungs that were *Mycl^{lox/lox}* or *Mycl^{+/+}* 4 mo after Ad-CGRP-Cre treatment. Data are representative of five mice per genotype examined. (D) Kaplan-Meier analysis showing increased survival in *Rb/p53/Pten; Mycl^{lox/lox}* mutants. *P*=0.0005 (log-rank). (E) Classification of major tumor types in mice from cohorts. (NSCLC) Non-SCLC. (F) Results of soft agar assay for the *Myc* family targeting CRISPR transfected SCLCs. (G) Quantification of soft agar assay. Colonies >0.20 mm in diameter were counted. *n*=3. Bars: B, 100 μ m; C, 500 μ m.

down-regulated genes in the preSC versus L-Myc-preSC comparison is shown in Figure 3A (see Supplemental Table 1 for the complete list of genes). Kyoto Encyclopedia

of Genes and Genomes (KEGG) pathway analysis of the L-Myc signature using DAVID (Database for Annotation, Visualization, and Integrated Discovery) bioinformatics

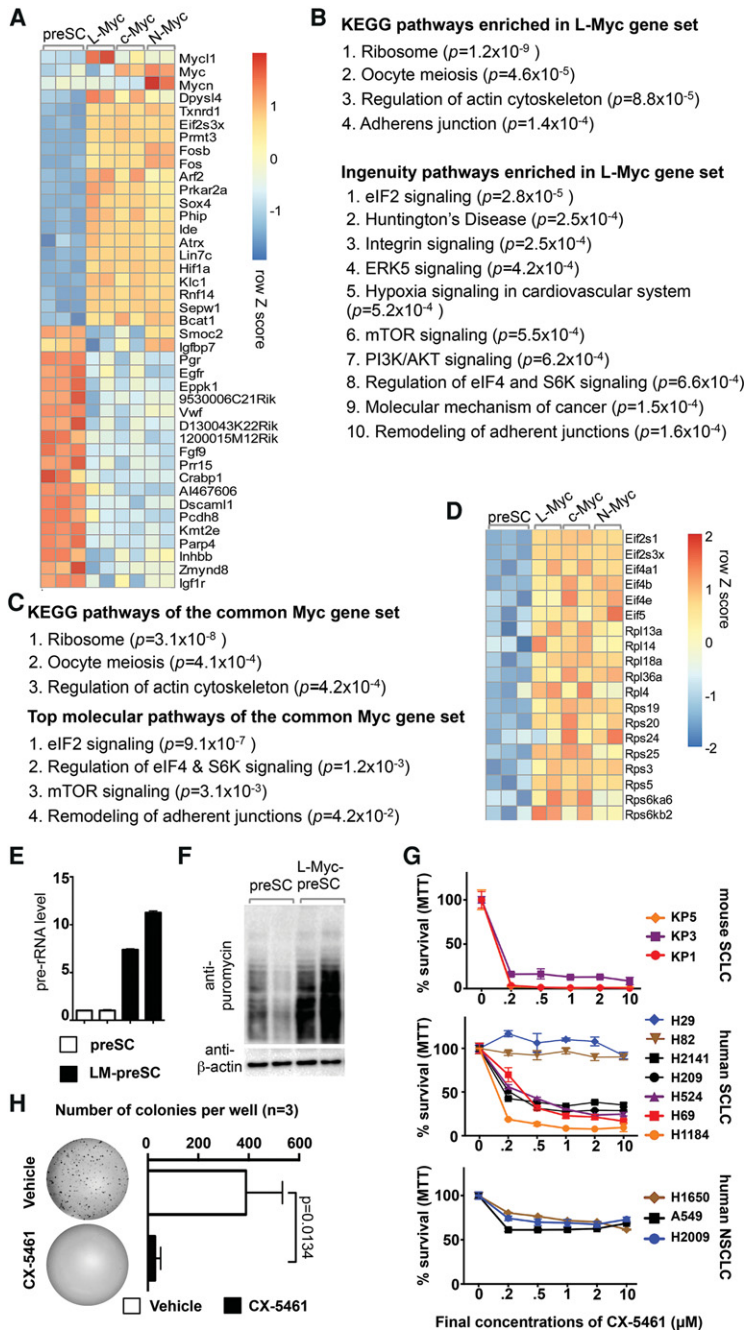


Figure 3. Overexpression of L-Myc promotes ribosomal transcription programs. (A) Heat map of the top 20 up-regulated and down-regulated genes between preSC and L-Myc-preSC. The right four columns of the heat map illustrate similar changes of the same genes in N-Myc-preSCs and c-Myc-preSCs. See the Materials and Methods for details of analysis. (B) Results of KEGG analysis and IPA showing the top molecular pathways related to the set of genes differentially regulated by L-Myc (L-Myc gene set). (C) Results of the same analyses as in B, showing the top molecular pathways related to the common Myc gene set. (D) Heat map of genes related to ribosome biogenesis. (E) Real-time PCR showing relative levels of pre-rRNA (ITS-1) of the 47S pre-rRNA relative to β 2 microglobulin in preSCs and L-Myc-PreSCs. (F) Western blot for puromycin incorporation in nascent proteins. Two-hundred-thousand cells were treated with 10 μ g of puromycin for 10 min. Actin is used as a loading control. (G) Results of MTT assay measuring the viability of cells treated with CX-5461 for 4 d. KP1, KP3, and KP5 are mouse SCLC cells, and H1650, A549, and H2009 are human non-SCLC cell lines. The rest of the cells above are human SCLC cell lines. These treatment and MTT assays were repeated with similar results at least once. (H) Results of soft agar assay for the mouse Rb/p53-deleted SCLC cells (KP1, KP3, and KP5) treated with 0.2 μ M CX-5461 (a RNA Pol I inhibitor) every 3 d for a month.

(National Institute of Allergy and Infectious Diseases/National Institutes of Health) indicated strong enrichment of pathways, including ribosome and adherens junction (Fig. 3B). Also, using Ingenuity Pathway Analysis (IPA; Ingenuity Systems), we found that the top molecular pathways significantly activated in the L-Myc signature include eIF2 signaling, regulation of eIF4 and p70S6K, and mTOR signaling—all known to control ribosome biogenesis and protein synthesis (Fig. 3B; see Supplemental Tables 2, 3 for the complete list of significant pathways identified). To differentiate common targets of the Myc family from L-Myc-specific targets, we also compared the L-Myc gene set with those regulated by N-Myc and

c-Myc and found 672 genes similarly altered in the preSCs transformed by the three Myc family members, which include the list of top up-regulated and down-regulated genes in the L-Myc set (Fig. 3A; Supplemental Table 1). The KEGG analysis and IPA of the common Myc gene set indicated significant enrichment of ribosome-related genes and the molecular pathways for ribosome biogenesis and protein synthesis, reflecting increased gene expression of ribosomal proteins and factors for ribosome assembly (Fig. 3C,D). Additionally, we tested whether L-Myc influences synthesis of ribosomal RNAs (rRNAs), as they are essential for ribosome biogenesis, and c-MYC has been shown to directly promote transcription

of ribosomal rRNA genes (Arabi et al. 2005; Grandori et al. 2005). Using qPCR, we measured pre-rRNA synthesis in preSCs or L-Myc-PreSCs. Because of rapid processing of pre-rRNA to mature rRNA, quantification of PCR products amplified using primers for the short-lived ITS-1 (internally transcribed spacer 1) of the 47S pre-rRNA can be used as a measure of the rate of rRNA synthesis. We found a striking up-regulation of pre-rRNA synthesis upon ectopic expression of L-Myc (Fig. 3E). Moreover, L-Myc overexpression also led to increased protein synthesis, as assessed by pulsing cells with puromycin prior to lysis and assessing puromycin incorporation into latent proteins by Western blot analysis (Fig. 3F). These results raise the possibility that L-Myc may promote tumor progression by up-regulating the protein synthesis machinery to meet increasing demand for structural proteins and various enzymes essential for dividing cells.

Modulation of ribosome biogenesis blocks SCLC progression and continuing growth

To test whether increased ribosome biogenesis reflects a L-Myc-associated vulnerability, we targeted the synthesis of rRNAs by inhibiting RNA Pol I. We used CX-5461, a specific inhibitor of RNA Pol I that prevents the association of RNA Pol I-specific initiation complex SL1 with DNA (Drygin et al. 2011). Four days of treatment with CX-5461 dramatically reduced the viability of three of three mouse SCLC cell lines from an *Rb/p53* Ad-CMV-Cre model as well as five of seven human SCLC lines in a dose-dependent manner, whereas several lung adenocarcinoma cell lines and two of seven SCLC cell lines responded only mildly to the drug at the same concentrations (Fig. 3G). The drug treatment also reduced the number of colonies formed by mouse SCLC cells in a soft agar assay (Fig. 3H). Gene expression analysis using RT-qPCR indicated that all of the mouse cells and these human SCLC cell lines sensitive to CX-5461 were associated with relatively higher levels of *MYCL* and *MYCN*, while the nonresponsive cells were associated with higher *MYC* (Fig. 1E; Supplemental Fig. S4A). Thus, in most SCLC cell lines, CX-5461 treatment reduced cell viability and the level of proliferation.

CX-5461 treatment suppresses SCLC in an autochthonous mouse model

We next tested the efficacy of CX-5461 in vivo using the autochthonous Ad-CMV-Cre *Rb/p53*-deleted model of SCLC (Meuwissen et al. 2003). This is an ideal preclinical model, as tumors emerge from lung neuroendocrine cells and undergo frequent metastasis and genetic alterations similar to human SCLC (Meuwissen et al. 2003; McFadden et al. 2014). Moreover, the *Rb/p53* model is a broadly generalizable system, given the near-universal deletion of *RB* and *P53* in human SCLC (George et al. 2015). Notably, CX-5461 is currently being tested in phase I clinical trials for leukemia, lymphoma, and myeloma (Australia clinical trials ID ACTRN12613001061729). Mice were monitored by MRI for tumor emergence and then entered into CX-

5461-treated or untreated groups when tumors of adequate size were detected. The CX-5461 dosage was 50 mg/kg orally every 3 d, a dosing regimen previously found to be well tolerated and efficacious in mouse lymphoma models (Drygin et al. 2011). All (nine of nine) untreated control mice exhibited progressive disease (PD) >25% over 2 wk (Fig. 4A–C). In contrast, only one of eight CX-5461-treated mice showed PD. We found stable disease (SD) upon CX-5461 treatment in five of eight animals and a partial response (PR) >25% reduction in three of eight cases (Fig. 4A–C). To examine target engagement, we collected tumors from mice treated for 2 wk or untreated, confirmed SCLC histology, and extracted RNA for real-time PCR analysis. We found a significant twofold reduction in preribosomal 47S RNA in tumors from the treated mice (Fig. 4D). Thus, SCLC suppression occurred with reduction in pre-rRNA synthesis. We also examined proliferation and cell death in treated tumors using BrdU analysis and immunohistochemistry. At 2 wk after CX-5461 treatment, we found significant decreases in BrdU-positive cells and pHH3 relative to untreated controls (Fig. 4E). In contrast, apoptosis levels, as assessed through cleaved caspase 3 immunostaining, were not significantly changed (Supplemental Fig. S4B). Thus, inhibition of RNA Pol I leads to suppressed proliferation upon treatment in vivo. We further performed gene set enrichment analysis (GSEA) using RNA sequencing (RNA-seq) data generated from untreated or treated mice to identify major biological pathways affected by CX-5461. We found strong reductions in MYC-related and cell cycle-related gene sets associated with CX-5461 treatment (Fig. 4G; Supplemental Table 4).

Discussion

A major challenge in SCLC is discerning which of the many commonly mutated genes are true drivers of tumor development. We report a novel system in which rare preneoplastic PNECs can be purified from mouse lungs in a sensitized SCLC model very early in tumor initiation. This system takes advantage of a mouse allele that uses the *Chromogranin A* (*Chga*) promoter to drive GFP expression in PNECs, which previous work has identified as the major SCLC cell of origin (Sutherland et al. 2011). Using this new approach, we can purify PNECs in the wild-type or mutant configuration. While we could not expand wild-type PNECs, PNECs deleted for *Rb/p53/p130* grow in culture and retain neuroendocrine features but do not grow as colonies in soft agar or form tumors when injected into immunocompromised mice. Overexpression of L-Myc, N-Myc, or c-Myc conferred the ability to grow in soft agar and form tumors that exhibit the histological features and markers of human SCLC. This model can now be applied to assess oncogenic and tumor-suppressive activity of many additional SCLC mutated genes.

It remains to be determined whether the preSCs represent a heterogeneous population of cells with differing tumor-initiating capacity. Although endogenous L-Myc

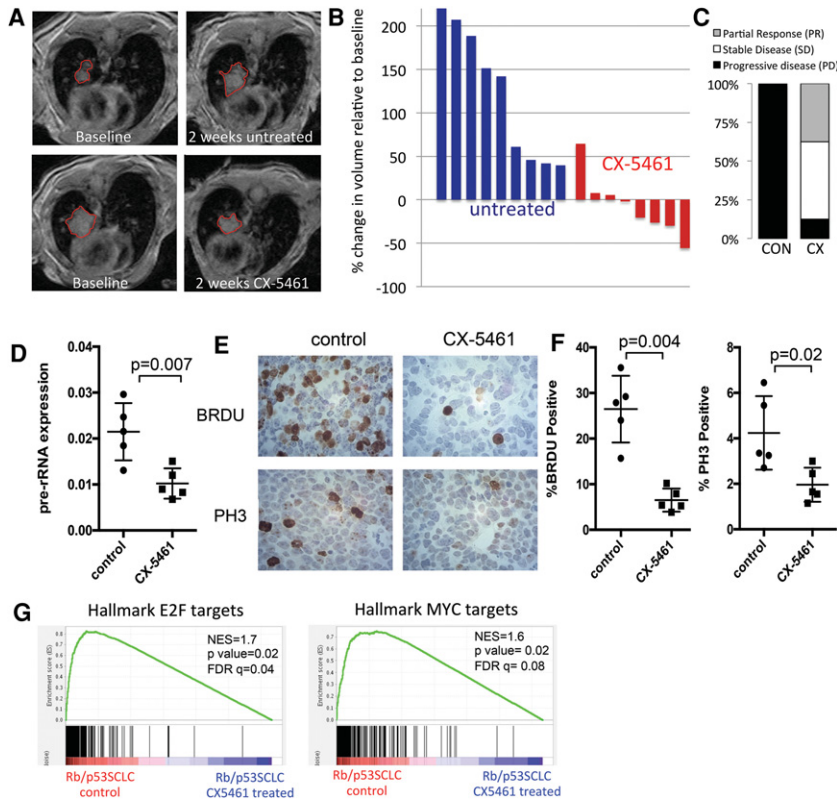


Figure 4. Inhibition of RNA Pol I suppresses SCLC in an autochthonous model. (A) Representative MRI images showing a baseline scan and the 2-wk time point. The tumor is outlined in red. (B) Waterfall plot showing tumor volume changes from baseline to the 2-wk time point quantified from an MRI in untreated (control) and CX-5461-treated mice. (C) Proportion of control and CX-5461-treated mice with PD, SD, or PR. (D) Real-time PCR showing relative levels of pre-rRNA (ITS-1) of the 47S pre-rRNA relative to $\beta 2$ microglobulin in tumors from control mice or undergoing 2 wk of CX-5461 treatment (E) BrdU and PH3 analysis of Rb/p53 tumors in untreated mice and mice treated for 2 wk with CX-5461 (F) Quantification of BrdU and PH3 levels from E. (G) GSEA enrichment plot using RNA-seq from five controls compared with five CX-5461-treated SCLC tumors. The 50-gene “hallmarks signatures” set from the Molecular Signatures Database (MSigDB) was queried. Supplemental Table 4 shows a complete set of significant gene sets differing in these conditions.

levels were low in the bulk preSC population compared with SCLC, single-cell analysis could reveal whether a subpopulation of preSCs express L-Myc. If so, it would be interesting to test for enhanced tumor-initiating capacity in this population. Alternatively, preneoplastic cells may undergo chromatin changes during SCLC tumor progression that results in increased L-Myc expression even without gene amplification. It is also possible that preSCs expanded under tissue culture conditions undergo changes in gene expression through the culturing process that contribute to the observed low expression of L-Myc. Future studies should compare FACS-sorted preSCs directly after sorting to assess similarities and differences in gene expression compared with the population of preSCs that expands in culture.

The effects of inactivating *Mycl* in two highly penetrant mouse models of SCLC were striking. The dramatic suppression of tumor development observed in the genetic model system suggested that inhibitory effects of *Mycl* loss were not simply owing to an inability to amplify the *Mycl* locus, an event that occurs in human SCLC and occasionally in the *Rb/p53/Pten* Ad-CGRP Cre model (Supplemental Fig. S3C). Instead, basal levels of *Mycl* are likely important for SCLC development. Thus, L-Myc-directed therapy may be more widely relevant to SCLC beyond the subset of patients that exhibit *MYCL* amplification.

Overexpression of L-Myc in the preSC system promoted rRNA transcription as well as mRNAs for ribosomal proteins. In a mouse model, E μ -MYC-driven lymphoma was

suppressed by hemizygous genetic deletion of ribosomal proteins (Barna et al. 2008), and the competitive advantage associated with dMYC expression in *Drosophila* was also abrogated by hemizygous mutations in ribosomal genes (de la Cova et al. 2004; Moreno and Basler 2004), genetic evidence that MYC-deregulated ribosomal biogenesis and cell growth may be important for pro-oncogenic function of all MYC family members. We interrogated the therapeutic potential of targeting this axis in SCLC by inhibiting RNA Pol I using the small molecule CX-5461. CX-5461 has been reported to exhibit efficacy in hematopoietic malignancies involving MYC (Devlin et al. 2016), and CX-5461 is being tested in clinical trials for leukemia and lymphoma. The efficacy of CX-5461 in autochthonous solid tumors models, however, has not been yet reported. Strikingly, CX-5461 was effective as monotherapy for *Rb/p53* mutant SCLC in an autochthonous model, as nine of nine untreated mice developed PD (>25% increase in tumor volume), but PD was seen in only one of eight CX-5461-treated mice. With CX-5461 treatment, either a PR (>25% decrease in tumor volume) or SD was found (Fig. 4A–C). SCLC is characterized by exquisite chemosensitivity followed by chemoresistance at recurrence. It will be critical to assess the extent to which RNA Pol I inhibition augments the response to chemotherapy in mouse models of SCLC. Interestingly, *MYC* family amplifications are far more frequent in SCLC cell lines derived from chemotherapy-treated versus chemo-naïve tumors, suggesting that very high levels of MYC family expression might contribute to chemoresistance (Johnson et al.

1987). An autochthonous L-Myc-overexpressing model (Huijbers et al. 2014) is one tool that can be used to determine the consequence of very high levels of L-Myc on the sensitivity to RNA Pol I inhibition.

Although MYC family proteins differ in the strength of their transcriptional and transforming activities, their interactions with other transcriptional regulators (Vo et al. 2016), and their developmental essentiality, the mutual exclusivity of amplifications in MYC family members in SCLC suggests that the mechanism of oncogenic activity among L-MYC, N-MYC, and c-MYC in SCLC is similar. We found that overexpression of any MYC family member could induce transcriptional programs associated with ribosomal biogenesis and protein translation (Fig. 3). Therefore, RNA Pol I inhibition may represent a therapeutic vulnerability relevant to SCLC exhibiting amplification in any MYC family member. We note that the MYC network is complex, and it is important that we better understand roles for other members of the network. For example, MAX is the dimerization partner for L-MYC and other MYC members and is the target of truncating mutations in a subset of SCLC (Romero et al. 2014). MAX binds other transcription factors in addition to MYC family members (for review, see Diolaiti et al. 2015), including MGA, a component of the network that is also inactivated in some SCLC samples (Romero et al. 2014). It remains to be determined how amplification or deletion in MYC members in SCLC shifts the composition of other MAX complexes in the broader MYC network and how inactivation of MAX in SCLC influences MYC signaling and protein synthesis control.

Previous studies have focused on the ability of CX-5461 to induce nucleolar stress and p53 activation in mediating *in vivo* efficacy (Bywater et al. 2012; Devlin et al. 2016). However, we found significant efficacy in p53-null SCLC, ruling out p53 activation as a relevant factor in the SCLC model. Our treatment of SCLC with CX-5461 *in vivo* was not associated with a strong apoptotic response. In SCLC, CX-5461 drove a p53-independent anti-proliferative effect associated with reduced E2F and MYC target gene expression (Fig. 4E–G). In one panel of 44 cell lines from multiple tumor types, there was no correlation between p53 genetic status and sensitivity to CX-5461 (Drygin et al. 2011). In contrast, p53 inactivation was clearly associated with reduced effects of CX-5461 in cell lines derived from an $E\mu$ -MYC mouse lymphoma model (Bywater et al. 2012). The importance of a p53-dependent anti-proliferative versus apoptotic response to CX-5461 likely differs across different tumor types, with effects in SCLC mediated by p53-independent anti-proliferative effects. Precisely how the anti-proliferative effects of CX-5461 in SCLC are mediated remains to be determined.

The protein translation machinery can be targeted at multiple levels beyond RNA Pol I inhibition, such as through inhibition of mTOR signaling or various EIF4F complex components that control translation initiation (Bhat et al. 2015). In SCLC, mTOR inhibition using everolimus was unsuccessful in a phase 2 clinical trial testing patients who failed first line therapy (Tarhini et al.

2010). Similarly, in the *Rb/p53* autochthonous mouse model, mTOR inhibition using the active site inhibitor AZD8055 lacked efficacy as monotherapy, although this treatment clearly enhanced the effects of a BCL2 inhibitor (Faber et al. 2015). In contrast, using the same *Rb/p53* autochthonous mouse model, we found that RNA Pol I inhibition was effective as monotherapy. Thus, RNA Pol I inhibition may represent a more direct strategy to inhibit the protein synthesis machinery. Our combination of genetic and pharmacological studies using a panel of genetically engineered mouse models reveal L-Myc signaling as a vulnerability and RNA Pol I inhibition as a promising therapeutic strategy for SCLC.

Materials and methods

We provide detailed methods in the Supplemental Material.

Mouse strains, Ad-Cre infection, and subcutaneous allografts

The SCLC mouse models bearing deletions in *p53*, *Rb*, *p130*, or *Pten* were previously described (Meuwissen et al. 2003; Schaffer et al. 2010; Cui et al. 2014). Construction of the *Mycl lox* strain and *Chga-GFP* transgenic strain expressing GFP under control of the *Chga* promoter is described in the Supplemental Material. All compound mice were maintained on a mixed background (129/SvJ; C57BL/6). Multiple cohorts of independent litters were analyzed to control for background effects. Ad-Cre was purchased from Vector Development Laboratory at Baylor College of Medicine (Ad-CMV-Cre) or the University of Iowa Gene Transfer Vector Core (Ad-CMV-Cre and Ad-CGRP-Cre). Intratracheal instillation of Ad-Cre was performed essentially as previously described (DuPage et al. 2009). For subcutaneous allografts, 1.0×10^5 mouse preneoplastic preSC cells or mouse tumor cells were injected in the flanks of immune-deficient nude mice (Harlan). Mice were maintained according to practices prescribed by the National Institutes of Health. All animal procedures were approved by the Animal Care and Use Committee at both the University of Virginia and the Fred Hutchinson Cancer Research Center, accredited by the Association for the Assessment and Accreditation of Laboratory Animal Care (AAALAC).

FACS analysis and sorting

Whole lungs or dissected lung tumors from the transgenic mice (*Chga-GFP*) that express GFP in lung neuroendocrine cells were minced and digested, rotating for 30 min in 25 U/mL Dispase (Gibco). Single-cell suspensions were stained with DAPI (Sigma) to visualize dead cells. GFP-positive live cells were sorted using BD Aria and FlowJo software (Tree Star, Inc.).

Protein synthesis assay

PreSC cells were pulsed with 10 μ g/mL puromycin and harvested 10 min later. Cells were lysed with Laemmli buffer, run on a 10% SDS-PAGE gel, transferred to PVDF membrane, and blotted with anti- β -actin (Santa Cruz Biotechnology, sc47778) or anti-puromycin (EMD Millipore, MABE343) antibodies.

Microarray analysis

RNA from cells or tumors was isolated using TRIzol (Invitrogen) and then purified using a RNeasy column (Qiagen) following

the manufacturer's protocol. The purified RNAs were processed and hybridized to Affymetrix Mouse Genome 430 2.0 expression array at the DNA Science Core at the University of Virginia. Array data have been uploaded to the Gene Expression Omnibus database (ID GSE77385). Detailed analysis methodology is described in the Supplemental Material.

Histology and immunostaining

Five-micrometer paraffin sections were used for H&E staining and immunostaining. For immunofluorescence, paraffin sections were dewaxed and rehydrated using Trilogy (Cell Marque) according to the manufacturer's instruction. The primary antibodies used were Synaptophysin (Neuromics, MO20000), pHH3 (Upstate Biotechnology, 06-570), Ki67 (BD Pharmingen, 550609), cleaved caspase 3 (Cell Signaling, 9661), UCHL1 (Sigma, HPA005993), CGRP (Sigma, c-8198), and anti-BRDU (BD Pharmingen). Alexa fluor-conjugated secondary antibodies (Invitrogen) were used for antibody detection, and anti-fade reagents with DAPI (Vector Laboratories) were used for preserving fluorescence and nuclear counterstaining. All microscopic images were acquired using a Nikon Eclipse Ni-U microscope. Image analysis and automated quantification were performed using NIS-Elements Basic Research (Nikon). Macroscopic images of lungs were acquired using an Olympus MVX10. Areas of tumors and whole lungs were quantified using ImageJ software. For quantification of the number of pHH3-positive cells, tumors of similar size and area were included. For pathological analyses, entire slides were digitally scanned at high (40 \times) resolution using the NanoZoomer 2.0 HT digital pathology system (Hamamatsu Photonics) and examined using the manufacturer's software. A pathologist (A.F. Gazdar) examined all of the scanned images in detail and captured multiple representative images. Terminology for neuroendocrine tumors was as described previously (Gazdar et al. 2015).

Animal imaging and tumor quantification

For therapeutic studies in the autochthonous model, *Rb^{lox/lox}; p53^{lox/lox}* mice were infected intratracheally with Ad-CMV-Cre. Mice were screened for detectable tumors between 8 and 14 mo following infection using a Bruker Icon small animal MRI. MRI covered the entire thoracic region at 1-mm intervals. We required that a tumor be present on at least three consecutive 1-mm slices for study entry. Typically, a single measurable tumor was detected, but, in cases with multiple tumors, the largest tumor was quantified. Tumor volume was measured using ImageJ.

Statistical analysis

Except where indicated otherwise, statistical significance was assayed by a Student's *t*-test with the Prism GraphPad software (two-tailed unpaired and paired *t*-test, depending on the experiment). Unless noted otherwise, pooled data are represented as the mean \pm SEM (standard error of mean). For the survival curve analysis and comparison, we used the Mantel-Cox test.

Acknowledgments

We thank Tyler Jacks (Koch Institute, Massachusetts Institute of Technology), Anton Berns (Netherlands Cancer Institute), and Hong Wu (University of California at Los Angeles) for *Rb^{lox}*, *p53^{lox}* and *Pten^{lox}* mice, respectively. We thank Jamie Nguyen and Jing-Shan Lim for help with MRI screening and retroviral

infection, respectively. We also thank Julien Sage and Andrew Hsieh for insightful comments on the manuscript. This work was performed partly with expert help from the Research Histology Core and DNA Science Core, which are supported by the University of Virginia Cancer Center (National Cancer Institute P30 Center Grant P30CA044579), and the Fred Hutchinson Cancer Research Center Histology Core and Genomics Core. This work was supported by a Uniting Against Lung Cancer Investigator grant (UALC-13-15), the American Cancer Society (RSG-15-066-01-TBG), and the National Cancer Institute (R01CA194461 to K.-S.P., R01CA181449 and R01CA148867 to D.M., and R01CA20525 to R.N.E.).

References

- Arabi A, Wu S, Ridderstrale K, Bierhoff H, Shiue C, Fatyol K, Fahlen S, Hydbring P, Soderberg O, Grummt I, et al. 2005. c-Myc associates with ribosomal DNA and activates RNA polymerase I transcription. *Nat Cell Biol* **7**: 303–310.
- Barna M, Pusic A, Zollo O, Costa M, Kondrashov N, Rego E, Rao PH, Ruggero D. 2008. Suppression of Myc oncogenic activity by ribosomal protein haploinsufficiency. *Nature* **456**: 971–975.
- Barrett J, Birrer MJ, Kato GJ, Dosaka-Akita H, Dang CV. 1992. Activation domains of L-Myc and c-Myc determine their transforming potencies in rat embryo cells. *Mol Cell Biol* **12**: 3130–3137.
- Bhat M, Robichaud N, Hulea L, Sonenberg N, Pelletier J, Topisirovic I. 2015. Targeting the translation machinery in cancer. *Nat Rev Drug Discov* **14**: 261–278.
- Birrer MJ, Segal S, DeGreve JS, Kaye F, Sausville EA, Minna JD. 1988. L-myc cooperates with ras to transform primary rat embryo fibroblasts. *Mol Cell Biol* **8**: 2668–2673.
- Bywater MJ, Poortinga G, Sanij E, Hein N, Peck A, Cullinane C, Wall M, Cluse L, Drygin D, Anderes K, et al. 2012. Inhibition of RNA polymerase I as a therapeutic strategy to promote cancer-specific activation of p53. *Cancer Cell* **22**: 51–65.
- Cui M, Augert A, Rongione M, Conkrite K, Parazzoli S, Nikitin AY, Ingolia N, Macpherson D. 2014. PTEN is a potent suppressor of small cell lung cancer. *Mol Cancer Res* **12**: 654–659.
- Dang CV. 2012. MYC on the path to cancer. *Cell* **149**: 22–35.
- de la Cova C, Abril M, Bellosta P, Gallant P, Johnston LA. 2004. *Drosophila myc* regulates organ size by inducing cell competition. *Cell* **117**: 107–116.
- Devlin JR, Hannan KM, Hein N, Cullinane C, Kusnadi E, Ng PY, George AJ, Shortt J, Bywater MJ, Poortinga G, et al. 2016. Combination therapy targeting ribosome biogenesis and mRNA translation synergistically extends survival in MYC-driven lymphoma. *Cancer Discov* **6**: 59–70.
- Diolaiti D, McFerrin L, Carroll PA, Eisenman RN. 2015. Functional interactions among members of the MAX and MLX transcriptional network during oncogenesis. *Biochim Biophys Acta* **1849**: 484–500.
- Drygin D, Lin A, Bliesath J, Ho CB, O'Brien SE, Proffitt C, Omori M, Haddach M, Schwaebe MK, Siddiqui-Jain A, et al. 2011. Targeting RNA polymerase I with an oral small molecule CX-5461 inhibits ribosomal RNA synthesis and solid tumor growth. *Cancer Res* **71**: 1418–1430.
- DuPage M, Dooley AL, Jacks T. 2009. Conditional mouse lung cancer models using adenoviral or lentiviral delivery of Cre recombinase. *Nat Protoc* **4**: 1064–1072.
- Faber AC, Farago AF, Costa C, Dastur A, Gomez-Caraballo M, Robbins R, Wagner BL, Rideout WM 3rd, Jakubik CT, Ham

- J, et al. 2015. Assessment of ABT-263 activity across a cancer cell line collection leads to a potent combination therapy for small-cell lung cancer. *Proc Natl Acad Sci* **112**: E1288–E1296.
- Gazdar AF, Savage TK, Johnson JE, Berns A, Sage J, Linnoila RI, MacPherson D, McFadden DG, Farago A, Jacks T, et al. 2015. The comparative pathology of genetically engineered mouse models for neuroendocrine carcinomas of the lung. *J Thorac Oncol* **10**: 553–564.
- George J, Lim JS, Jang SJ, Cun Y, Ozretic L, Kong G, Leenders F, Lu X, Fernandez-Cuesta L, Bosco G, et al. 2015. Comprehensive genomic profiles of small cell lung cancer. *Nature* **524**: 47–53.
- Grandori C, Gomez-Roman N, Felton-Edkins ZA, Ngouenet C, Galloway DA, Eisenman RN, White RJ. 2005. c-Myc binds to human ribosomal DNA and stimulates transcription of rRNA genes by RNA polymerase I. *Nat Cell Biol* **7**: 311–318.
- Hatton KS, Mahon K, Chin L, Chiu FC, Lee HW, Peng D, Morgenbesser SD, Horner J, DePinho RA. 1996. Expression and activity of L-Myc in normal mouse development. *Mol Cell Biol* **16**: 1794–1804.
- Huijbers IJ, Bin Ali R, Pritchard C, Cozijnsen M, Kwon MC, Proost N, Song JY, de Vries H, Badhai J, Sutherland K, et al. 2014. Rapid target gene validation in complex cancer mouse models using re-derived embryonic stem cells. *EMBO Mol Med* **6**: 212–225.
- Johnson BE, Ihde DC, Makuch RW, Gazdar AF, Carney DN, Oie H, Russell E, Nau MM, Minna JD. 1987. myc family oncogene amplification in tumor cell lines established from small cell lung cancer patients and its relationship to clinical status and course. *J Clin Invest* **79**: 1629–1634.
- Kc W, Satpathy AT, Rapaport AS, Briseno CG, Wu X, Albring JC, Russler-Germain EV, Kretzer NM, Durai V, Persaud SP, et al. 2014. L-Myc expression by dendritic cells is required for optimal T-cell priming. *Nature* **507**: 243–247.
- McFadden DG, Papagiannakopoulos T, Taylor-Weiner A, Stewart C, Carter SL, Cibulskis K, Bhutkar A, McKenna A, Dooley A, Vernon A, et al. 2014. Genetic and clonal dissection of murine small cell lung carcinoma progression by genome sequencing. *Cell* **156**: 1298–1311.
- Meuwissen R, Linn SC, Linnoila RI, Zevenhoven J, Mooi WJ, Berns A. 2003. Induction of small cell lung cancer by somatic inactivation of both Trp53 and Rb1 in a conditional mouse model. *Cancer Cell* **4**: 181–189.
- Moreno E, Basler K. 2004. dMyc transforms cells into super-competitors. *Cell* **117**: 117–129.
- Nakagawa M, Takizawa N, Narita M, Ichisaka T, Yamanaka S. 2010. Promotion of direct reprogramming by transformation-deficient Myc. *Proc Natl Acad Sci* **107**: 14152–14157.
- Nau MM, Brooks BJ, Battey J, Sausville E, Gazdar AF, Kirsch IR, McBride OW, Bertness V, Hollis GF, Minna JD. 1985. L-myc, a new myc-related gene amplified and expressed in human small cell lung cancer. *Nature* **318**: 69–73.
- Romero OA, Torres-Diz M, Pros E, Savola S, Gomez A, Moran S, Saez C, Iwakawa R, Villanueva A, Montuenga LM, et al. 2014. MAX inactivation in small cell lung cancer disrupts MYC-SWI/SNF programs and is synthetic lethal with BRG1. *Cancer Discov* **4**: 292–303.
- Rudin CM, Durinck S, Stawiski EW, Poirier JT, Modrusan Z, Shames DS, Bergbower EA, Guan Y, Shin J, Guillory J, et al. 2012. Comprehensive genomic analysis identifies SOX2 as a frequently amplified gene in small-cell lung cancer. *Nat Genet* **44**: 1111–1116.
- Schaffer BE, Park KS, Yiu G, Conklin JF, Lin C, Burkhardt DL, Karnezis AN, Sweet-Cordero EA, Sage J. 2010. Loss of p130 accelerates tumor development in a mouse model for human small-cell lung carcinoma. *Cancer Res* **70**: 3877–3883.
- Sutherland KD, Proost N, Brouns I, Adriaensen D, Song JY, Berns A. 2011. Cell of origin of small cell lung cancer: inactivation of Trp53 and Rb1 in distinct cell types of adult mouse lung. *Cancer Cell* **19**: 754–764.
- Tarhini A, Kotsakis A, Gooding W, Shuai Y, Petro D, Friedland D, Belani CP, Dacic S, Argiris A. 2010. Phase II study of everolimus (RAD001) in previously treated small cell lung cancer. *Clin Cancer Res* **16**: 5900–5907.
- van Riggelen J, Yetil A, Felsher DW. 2010. MYC as a regulator of ribosome biogenesis and protein synthesis. *Nat Rev Cancer* **10**: 301–309.
- Vo BT, Wolf E, Kawauchi D, Gebhardt A, Rehg JE, Finkelstein D, Walz S, Murphy BL, Youn YH, Han YG, et al. 2016. The interaction of Myc with Miz1 defines medulloblastoma subgroup identity. *Cancer Cell* **29**: 5–16.